# Miniature Fourier Transform Instrument for Radiation Thermometry

## Franklin J. Dunmore and Leonard M. Hanssen

*Optical Technology Division, National Institute of Standards and Technology (NIST), Gaithersburg MD 20899*

A miniature Fourier transform (FT) spectrometer has been tested as a device for remotely measuring the temperature of a high stability/emissivity blackbody. The commercially manufactured device is based on the novel design of a polarizing Wollaston prism spatial domain interferometer, with a Si diode array detector, and without any moving parts. The measurement of temperature using Planck's law showed a consistent nonlinear effect. This results in an error of the order of 1% for measurement of temperatures 500 K and above. Planned calibration measurements should reduce the nonlinearity related error and improve the FT temperature measurement.

## INTRODUCTION

Fourier transform spectrometry over a broad spectral range (using Planck's Radiation Law) shows promise for allowing accurate, contact-free temperature measurement and a Planck's Law based Kelvin Temperature scale[1]. Advances in fast temporal scan FT spectroscopy promise much shorter measurement time compared to the standard dispersive methods of thermal radiometry. To further these possibilities a commercially manufactured (by Photonex Ltd. (2,3)) Wollaston prism polarizing type miniature Fourier transform spectrometer (MFTS) has been tested to measure the temperature of high stability/emissivity blackbodies (4). The MFTS in this report uses a Si diode array detector sensitive in the 200 nm to 1100 nm (9000 $cm^{-1}$ to 50000 $cm^{-1}$) wavelength region. For blackbody sources at 2000 K, only millisecond data acquisition time is necessary. This makes the MFTS a potentially useful device where fast measurements are required.

## THE INSTRUMENT

Shown in Fig. 1 is a schematic of the MFTS which is based on the design of Padgett, et al. (5). From left to right, the first element is a linear polarizer oriented at 45° with respect to the plane of the paper. In the center is a Wollaston prism which is an optical combination of two wedged birefringent calcite slabs with their optical axes oriented perpendicular to each other. This acts as a beam splitter for the light coming from the polarizer. For the polarization component parallel to the optical axis, the refractive index at 589 nm is $n_o$=1.658; for the perpendicular component it is $n_e$=1.486. For a ray crossing the prism at the center $d$=0, the induced optical path length difference between the two beams in the first wedge is compensated in the second, resulting in a net zero difference. For $d \neq 0$, the two beams will traverse differing optical path lengths. The focusing optics will recombine the rays at the 1024 element Si diode array.
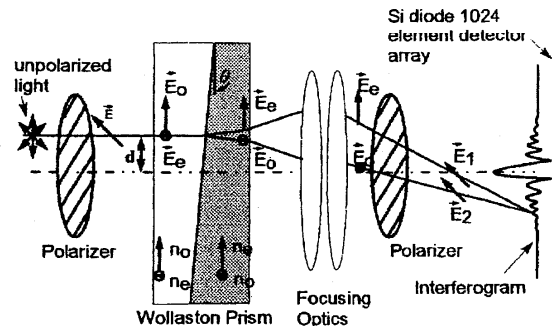


Figure 1. The optical layout of the MFTS.

All wavelengths interfere constructively for $d$=0 at the array leading to the central maximum of an interferogram in the spatial domain. Where $d \neq 0$ there will be modulation of the intensity according to

$$I(v) \propto |A(v)|^2 (1 + \cos(2\pi\Delta v)) \qquad (1)$$

where $A$ is the Electric field amplitude, $v$ is the wavenumber and

$$\Delta = 2d(n_e - n_o)\tan\theta \qquad (2)$$

is the path length difference, with $\theta$ the prism wedge angle (5). The accompanying instrument software takes the Fourier transform of the spatial fringe pattern (interferogram) to give the instrument spectral signal $S(v)$ as a function of wavenumber. In addition, the software applies

corrections for the wavenumber variation of the refractive indices and polarizer efficiencies. The wavelength range of the polarizers limit the wavelengths that are modulated by the prism. For this instrument they cut off at 600 nm. The long wavelength cutoff of the Si diode array detector is at a wavelength less than 1100 nm. This results in an operational range of 9000 cm$^{-1}$ to 16700 cm$^{-1}$ (1100 nm to 600 nm) with a full width at half maximum resolution of 27 cm$^{-1}$ for the instrument, determined primarily by the number of pixels of the Si diode array (5).

All expanded uncertainties in this report have a coverage factor $k$=2 (95% confidence) (6). The expanded uncertainty in the wavenumber, 10 cm$^{-1}$, is estimated to be less than half of resolution limit for this instrument. This uncertainty can be reduced by calibration with a stable laser source (5).

## RESULTS AND ANALYSIS

To test its capability for radiometric temperature measurement the MFTS was set up to view a pyrolitic graphite cavity blackbody with an emissivity of 99.9% (7) made by VIINOFI (8). The temperature of the blackbody was measured using a NIST standard pyrometer, calibrated against a gold fixed point blackbody source. The 0.4 mrad (full angle) field of view of the MFTS was limited by a 0.2 mm aperture placed at the end of a baffle tube. The expanded uncertainty of the pyrometer measurement is 3.14 K (9). The following resullts are representative only for this particular device at this particular time.

The resulting MFTS spectra of the blackbody source at five temperatures ranging from 1500 K to 2500 K are shown in Fig. 2. The spectral shape of the signal $S$ is due to a combination of the blackbody spectrum, the polarizer efficiencies and the Si diode responsivity. As the temperature increases, the signal increases rapidly,
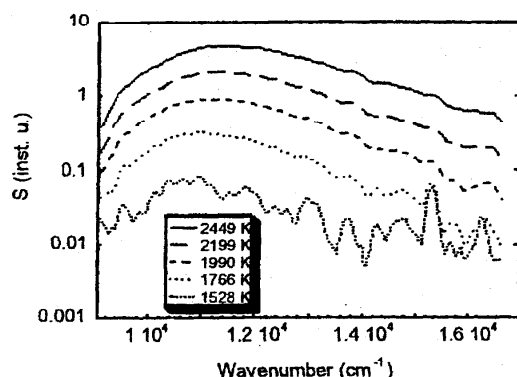


**Figure 2.** Spectral signal $S$ in instrumental units, versus wavenumber for several blackbody source temperatures.

consistent with Planck's Law and the peak signal shifts to higher frequencies consistent with Wien's displacement Law. At the lower temperatures, a reproducible fine

structure of small amplitude, common to all of the curves becomes apparent. This is due to a combination of the variability and nonlinearity of each pixel's responsivity.

Initially we assume linear response. Then a simple calibration procedure can be performed in order to measure temperature. First the instrument spectral signal $S(v,T)$ is measured for a blackbody source at several temperatures measured by the NIST standard pyrometer. Then the theoretical spectral flux $\Phi_v(v,T)=A\Omega L_v(v,T)$ is calculated at one calibration temperature $T_0$. Here $A$ is the effective area of the blackbody source (determined by aperture size), $\Omega$ is the solid angle subtended by the detector array, and the Planckian spectral radiance $L_v$ is given by:

$$L_v(v,T) = \frac{c_1 n^2 v^3}{\exp(c_2 v/T) - 1} \qquad \text{(W sr}^{-1}\text{m}^{-1}\text{)}^{\dagger} \qquad (3)$$

where $T$ is the true temperature measured by the NIST pyrometer. The constants are $c_1$=1.191 × 10$^{-16}$ W sr$^{-1}$ m$^2$, $c_2$=1.439 × 10$^{-2}$ K m (10) and $n$=1.00028 is the refractive index of air at 1 μm (11). Then the instrument spectral responsivity function $R$ is calculated at the calibration temperature $T_0$:

$$R(v) = \frac{S(v,T_0)}{\Phi_v(v,T_0)} \qquad (4)$$

Then the spectral flux $\Phi_{cv}$ calibrated to $T_0$ by Equation 4, at a different temperature $T'$ is

$$\Phi_{cv}(v,T') = \frac{S(v,T')}{R(v)} \qquad (5)$$

where $T'$ can be any other of the several temperatures of Fig. 2. Therefore the spectral flux can be deduced at any other temperature by using Eq. (4). Finally $\Phi_{cv}(v,T')$ is fitted to the Planckian theoretical spectral flux $\Phi_v(v,T')$ for the single parameter $T'$. It is expected that the deduced temperature $T'$ should equal the true temperature $T$ to within the expanded uncertainty of the pyrometer measurement, 3.14 K. However, it has not been the case and the reasons are discussed below.

In Fig. 3 the dashed lines are the Planckian spectral fluxes at the true temperatures, which are shown to the right, the dots are the calibrated spectral fluxes $\Phi_{cv}$, and the solid lines are the fits of Planck's Law to $\Phi_{cv}$ with the temperature values shown to the left. The differences between the fitted temperatures and the true temperatures are shown in the middle. In Fig. 3, 2449 K is the calibration temperature and

416

the expanded uncertainty is less than 2 K for the temperature fits to $\Phi_{cv}$. There is a systematic error in the measured temperature, on the order of 1% of the temperature, that decreases with decreasing temperature differences from the calibration temperature.

In order to ascertain the discrepancy between measured and deduced temperatures, we have measured the spectral responsivity function $R$ at various temperatures of the blackbody. Shown in Fig. 4 is $R$ versus wavenumber, derived from the data of Fig. 2, for several temperatures ranging from 2000 K to 2500 K. There is a significant deviation from linear spectral responsivity, which is apparent from the variation of $R$ with temperature and therefore incident spectral flux. Interestingly, this nonlinear
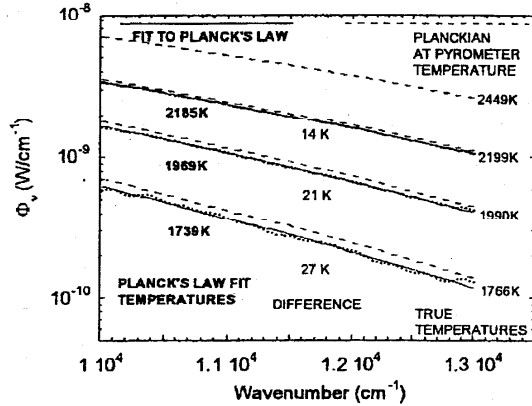


Figure 3. Logarithmic plot of calibrated spectral flux $\Phi_{cv}$ from data (dots), calculated spectral flux $\Phi_V$ (thin line), and the Planck's Law fits to $\Phi_{cv}$ (solid line).

behavior is opposite to the more common decrease in responsivity as the incident flux reaches a saturation value. Instead, $R$ increases as the flux increases. This is readily apparent in Fig. 5, where $R$ versus $\Phi_V$ is plotted for several frequencies. For linear responsivity, $R$ should be a constant. For each curve the first data point to the left (at the lowest spectral flux) is $T = 1766$ K, the second to the right is for 1990 K, the third is for 2199 K and the last is for 2449 K. The data, replotted in Fig. 6 between $S$ and $\Phi_V$, is best represented as a cubic polynomial. The slope of the $S$ versus $\Phi_V$ curve is approximately the responsivity and is strongly wavenumber dependent.

The expanded uncertainty for $S$ is less than 0.3%. For the $\Phi_V$ and $\Phi_{cv}$ scales in Fig. 3, the $\Phi_V$ scale in Figs. 5.and 6, and the $R$ scale in Figs. 4 and 5, it is 5%. The uncertainty for the $\Phi_V$ and $\Phi_{cv}$ scales is dominated by the uncertainty of the area of the aperture and does not contribute to the uncertainty of the measured temperatures derived below because it has no effect in the process of fitting $\Phi_{cv}(v, T')$ for $T'$. This is because the $\Phi_V$ and $\Phi_{cv}$ scale uncertainties are independent

of temperature and it is the shape of the curve, not the absolute spectral flux level that determines the fit for $T'$.

The cause of the instrumental nonlinear responsivity is most likely nonlinearity of the Si diode detector array. This nonlinear responsivity is due to stray capacitance in the sample and hold circuit of the array connecting each pixel to
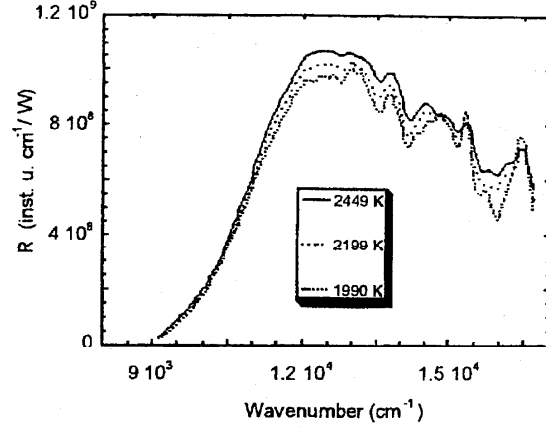


Figure 4. MFTS spectral responsivity $R$ versus wavenumber for three blackbody temperatures.

the A/D converter; it is more prevalent in diode array detectors than in single diode detectors (12).

The MFTS temperature measurement is extremely sensitive to nonlinearity because, for the wavenumber and temperature ranges described in this report, the incident spectral flux has a very strong dependence on temperature. This can be seen in the following relation between the fractional changes of $\Phi_V$ and $T$:

$$\frac{\Delta\Phi_v}{\Phi_v} = \frac{c_2 v}{T}\left(1 - e^{\frac{c_2 v}{T}}\right)^{-1} \cong 8.6\frac{\Delta T}{T} \qquad (6)$$

This corresponds approximately to a ninth-power temperature dependence of the spectral flux in this wavenumber-temperature regime. The nonlinearity can be described by relating $S$ to $\Phi_V$ by

$$S = a + b\Phi_v + c\Phi_v^2 + d\Phi_v^3 \qquad (7)$$

The $S$ offset, due to dark current in the Si diode pixels is $a \cong 0.01$. In the linear case $c=d=0$ and $R=(S-a)/\Phi$.

The data of Fig. 6 is fit to Eq. (7), and the result is shown in an inset to Fig. 6. The 12000 cm$^{-1}$ to 13000 cm$^{-1}$ wavenumber range is the region of maximum combined responsivity of the MFTS. Here the values of $b$, $c$, and $d$ are relatively wavenumber independent. Eq. (7) can be inverted to give $\Phi_V$ as a function of $S$ for a single wavenumber. When data is calibrated this way, better agreement with the NIST pyrometer is found, where the differences between the true temperatures and the temperatures of the fits to Planck's
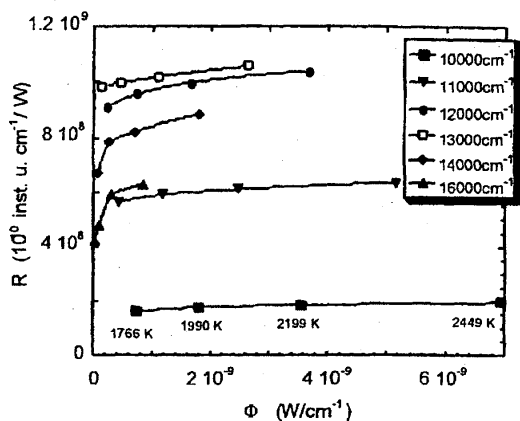
**Figure 5.** Spectral responsivity $R$ versus incident spectral flux $\Phi_v$ at several wavenumbers spanning the spectral range of the MFTS.
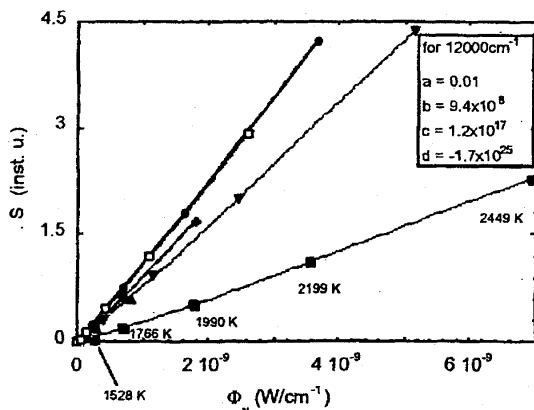


**Figure 6.** MFTS spectral signal $S$ versus incident spectral flux $\Phi_v$. The legend is the same as in Figure 5.

Law, as in Fig. 3, are 4 K for $T=1766$ K, 1 K for $T=1990$ K and 3 K for $T=2199$ K. The last two temperatures came within the expanded uncertainty of the NIST pyrometer, 3.14 K.

Attempts to recalibrate the spectrometer across its entire spectral range proved unsuccessful because the variation of the spectral responsivity has a strong wavenumber dependence as is seen for the sample of frequencies across the MFTS spectral range in Figs. 5 and 6. $S$ at any one wavenumber is determined by the spectral responsivity at all wavenumbers of every pixel of the Si diode detector array. This makes detector linearization by recalibrating $S$ over a broad spectral range difficult. It will be necessary to correct the interferogram directly prior to Fourier transform processing, in order to increase the radiometric accuracy of the MFTS temperature measurement.

## CONCLUSIONS AND FUTURE WORK

The MFTS is a very useful device for spectral radiometry because of its speed and compact portable nature. However, its accuracy for temperature measurements is limited by the nonlinear behavior of its detector array. This may be remediable. An effective method for detector linearization in FT spectrometry has been developed for standard FT instruments used with nonlinear detectors, such as HgCdTe. The measured interferogram, is corrected via a calibrated responsivity curve obtained by comparison to a NIST transfer-standard linear Ge detector (13). For the case of the MFTS, each pixel of the bare Si diode array will have to be characterized with respect to a standard Si detector. When the interferogram is calibrated for individual pixel non-linearity, the resulting spectrum after Fourier transformation should have significantly reduced detector nonlinearity effects and the temperature measurement accuracy will be limited by other sources of error such as wavenumber scale uncertainty and deviations from ideal behavior of the polarizer and prism, which can be further investigated.

## REFERENCES

1. H .A. Gebbie, R. A. Bohlander, and R.P. Futrelle, Nature 240, 391 (1972): H .A. Gebbie, Infrared Phys. 34 , 575 (1993).
2. The mention of manufacturers and model names is intended solely for the purpose of providing technical information useful to the reader and in no way should be construed as an endorsement of the named manufacturer or product.
3. Photonex Ltd., 35 Cable Depot Road, Riverside Industrial Estate, Clydebank, Glasgow G81 1UY United Kingdom
4. F.J. Dunmore et al., 25th Anniversary Conference of the Council for Optical and Radiation Measurements (1997).
5. M.J. Padgett et al, Applied Optics 33, 6035 (1994).
6. B.N. Taylor and C.E. Kuyatt, Guidelines for Evaluating and Expressing the Uncertainty of NIST Measurement Results, NIST Technical Note 1297, 1994 Edition, pp 2-6.
7. V.I. Sapritsky and A.V. Prokhorov, Appl. Opt., 34, 5645 (1995).
8. All Russian Institute for Optical and Physical Measurements, Moscow, Russia.
9. NIST Special Publication, 1997, (in press).
10. P.R. Griffiths and J. A. de Haseth, Fourier Transform Infrared Spectroscopy, New York: John Wiley & Sons, 1986, ch. 7, p. 248.
11. B. Edlen, Metrologia, 2, 71 (1966).
12. Conversations with Bill Beckman, Mark Hollbrook and Andy Smith (Photonex LTD).
13. Z.M. Zhang, C.J. Zhu, and L.M. Hanssen, Applied Spectroscopy 51, 576 (1997).